TABLE V

PERFORMANCE OF THE CLASSIFIER USING EGM_{RA} AND EGM_{RV} (VT VS. VF)

	VF	VT
Shock	TP = 223	FP = 1
Pacing	FN = 26	TN = 189
	Sensitivity = 89.6%	Specificity = 99.5%

choose the χ^2 statistics due to its lower computational cost.

Once a life-threatening arrhythmia is detected, the ICD must apply a shock, if rhythm is a VF, or start pacing, if rhythm is a VT. During a VF, the EGMs have higher frequencies and are desynchronized; therefore, the dispersion of one ventricular EGM against the another is high. Using a two-dimensional histogram of two ventricular EGMs, or of two EGMs from the right heart, the dispersion was extracted from the deviation of the frequency in each of the bins.

A 10-fold cross-validation showed that the method has a high sensibility and specificity even in the separation of SVTs from VTs when using ventricular EGMs. However, EGMs of both ventricles are not usually acquired in dual-chamber ICDs. The results of the classification using EGMs from the right heart showed a poor separation of SVTs and VTs. These results are expected to be improved when accounting information from past windows. For instance, during a SVT if some isolated samples was classified as VT, the classification as a VT is probably wrong. The low standard deviation of the threshold during the cross validation reflects the stability of the chosen indices.

These results were obtained from a limited data set. The algorithm must be evaluated in more data from different conditions. The use of indices obtained from histograms has the advantage to be independent of the signal amplitude. Therefore, it is expected to be more robust, for example, to differences among patients and to patients activities.

V. CONCLUSIONS AND FUTURE WORKS

In a limited dataset, this preliminary study showed the possibility to detect life-threatening arrhythmias from the comparison of simultaneous electrograms by the extraction of the independence of electrograms using the χ^2 statistic and of the relative dispersion of electrograms using the standard deviation of their joint probability.

. In future studies, other features should be extracted from the EGM_{RV} and EGM_{RA}, such as phase synchronization and delay or relative period, in order to improve the classification using EGMs from the right heart only, which would permit the application of this algorithm not only in biventricular ICDs but also in dual-chamber ICDs.

REFERENCES

[1] "State-specific mortality from sudden cardiac death - united states, 1999," *MMWR Weekly February 15*, vol. 51, no. 06, pp. 123–126, 2002.

[2] C. W. Israel, "How to avoid inappropriate therapy," *Current Opinion in Cardiology*, vol. 23, p. 65.71, 2008.

[3] A. Cebrian, J. Millet, and F. Castells, "Implantable cardioverter defibrillator algorithms: status review in terms of computational cost," *Biomed Tech (Berl)*, vol. 52, no. 1, pp. 25–30, 2007.

[4] P. A. Friedman, R. L. McClelland, W. R. Bamlet, H. Acosta, D. Kessler, T. M. Munger, N. G. Kavesh, M. Wood, E. Daoud, A. Massumi, C. Schuger, S. Shorofsky, B. Wilkoff, and M. Glikson, "Dual-chamber versus single-chamber detection enhancements for implantable defibrillator rhythm diagnosis the detect supraventricular tachycardia study," *Circulation*, vol. 113, no. 25, pp. 2871–2879, 2006.

[5] E. Aliota, R. Nitzsche, and A. Ripart, "Arrhythmia detection by dual-chamber implantable cardioverter defibrillators: A review of current algorithms," *Europace*, vol. 6, pp. 273–286, 2004.

[6] D. A. Theuns, M. Rivero-Ayerza, E. Boersma, and L. Jordaens, "Prevention of inappropriate therapy in implantable defibrillators: A meta-analysis of clinical trials comparing single-chamber and dual-chamber arrhythmia discrimination algorithms," *International Journal of Cardiology*, vol. 125, no. 3, pp. 352 – 357, 2008.

Circ J 2009; **73:** 1395–1396

Coronary Artery Volume Noninvasively Measured With Multislice Computed Tomography

— Definition, Accuracy and Implication —

Masaru Sugimachi, MD; Toru Kawada, MD

In this issue of *Circulation Journal*, Ehara et al[1] describe a new concept of measuring 'coronary artery volume' (CAV) to examine the balance between coronary vasculature and myocardial mass. They have developed a method of measuring CAV as accurately as possible using 64-slice computed tomography (64-MSCT). An adaptive threshold value was used to detect the coronary artery border to improve the accuracy of CAV. Ehara et al have exemplified the usefulness of CAV by examining the relationship between CAV and left ventricular mass (LVM) in consecutive patients undergoing MSCT without significant coronary artery stenosis or left ventricular wall motion abnormality. The authors concluded that CAV increases with LVM, but that the increase was not sufficient for the increase in LVM.

Article p 1448

What is CAV?

The authors have defined CAV as the sum of the small volumes opacified by the contrast medium. The opacified small volumes were detected by the difference of radiodensity or Hounsfield unit (an index showing the degree of transparency to X-ray) using 64-MSCT (see below for details). Because the authors have analyzed data of routine 64-MSCT for the evaluation of coronary artery disease, the image is taken when the arterial side is mainly opacified, during the diastolic cardiac phase, and under coronary vasodilatation. Therefore, CAV mainly represents the sum of volumes of epicardial coronary arteries larger than the arteries undetectable due to the limited resolution of MSCT (see below).

How Accurate and Reproducible is CAV Measurement?

In this article, the authors have established a method of measuring CAV with every attempt to improve the accuracy and reproducibility for their MSCT device. These procedures are worthy of being discussed for other researchers who are interested in and would like to reproduce CAV measurement.

Inaccuracies and variability of CAV measurement would arise from (1) an arbitrary cut-off value for border detection, (2) partial volume effect, (3) motion artifact and (4) possible variable resolution of various MSCT devices. The authors have wisely minimized the errors introduced by the first 3 factors.

It is usually difficult to determine the border of the coronary arteries with a reasonable criterion. This may be because opacification of arteries is incomplete, or the opacification is thinner near the border than the center, resulting in a gradual decrease in radiodensity at the border, rather than a clear-cut abrupt change in radiodensity. In addition, at the border of small arteries, a voxel (the smallest size identified by 64-MSCT) may contain both arterial lumen (which is opacified) and arterial wall (which is not opacified). A voxel has a radiodensity of an intermediate value between an opacified and unopacified voxel, which is known as the 'partial volume effect'.

To minimize the errors introduced by an arbitrary cut-off value and the partial volume effect, the authors have developed a way of reasonably determining the cut-off value for border detection, based on preliminary phantom experiments with moving cylinders containing various concentrations of contrast medium. The results of these preliminary experiments are summarized in Figures 1–3 in Ehara et al! Figure 2 clearly shows that a cut-off value that exactly reproduces the phantom cylinder volume can be determined. The cut-off value is, however, not fixed, but changes with the true radiodensity of the contrast medium in the cylinder. Based on this, the authors determined the cut-off value for CAV measurement, adaptively in each subject, in reference to the radiodensity of the proximal region of the left and right coronary arteries. The cut-off value was not relatively influenced by different heart rates, which also decreased the degree of error by motion artifacts. Similar procedures may be applicable to quantitative coronary angiography.

The determined threshold is, however, only valid for the specific MSCT device used in the study by Ehara et al! If other researchers are to reproduce their CAV measurement, another attempt to determine the threshold for their device is necessary.

The limited resolution of MSCT would determine the definition of CAV. The authors used MSCT with an isotropic resolution of 400μm. This indicates that CAV in the paper by Ehara et al would be the sum of volume of the arteries >400μm. If MSCT is used with a different resolution, the definition of CAV would be different and CAV would be systematically different.

(Received June 17, 2009; accepted June 17, 2009)

Department of Cardiovascular Dynamics, Advanced Medical Engineering Center, National Cardiovascular Center Research Institute, Suita, Japan

Mailing address: Masaru Sugimachi, MD, Department of Cardiovascular Dynamics, Advanced Medical Engineering Center, National Cardiovascular Center Research Institute, 5-7-1 Fujishirodai, Suita 565-8565, Japan. E-mail: su91mach@ri.ncvc.go.jp

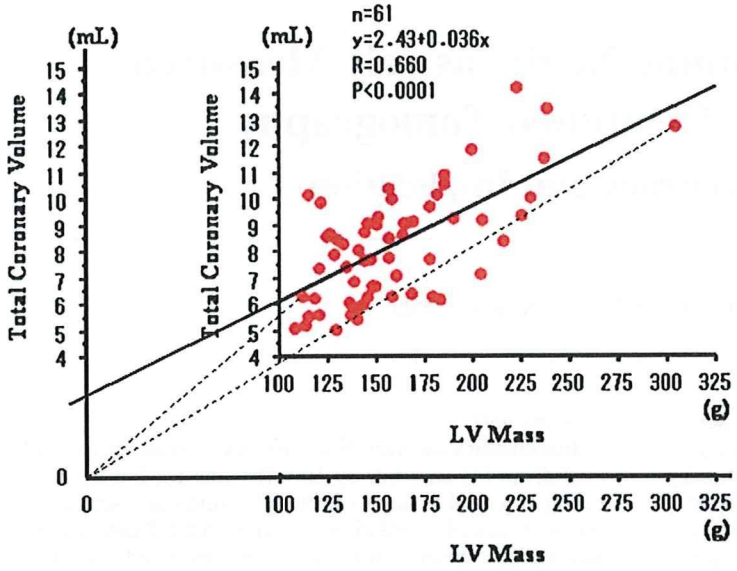

Figure. Linear regression between coronary artery volume (total coronary volume) and left ventricular (LV) mass (reproduced and modified from Ehara et al[1]). The axes are extended and the regression line is extrapolated to show a positive offset of coronary artery volume. Schematically, the authors have compared the slopes of dashed lines.

Is CAV a Proxy for Capillary Density or Coronary Flow Reserve?

The relation between coronary vasculature and myocardial mass, or more specifically inappropriate perfusion of the myocardium, has been traditionally examined histologically[2] by capillary density. Later, similar information was obtained in vivo by the measurement of coronary flow reserve. In fact, some have described the relationship between coronary capillary density and coronary flow reserve in patients with hypertrophic cardiomyopathy[3], in patients with idiopathic dilated cardiomyopathy[4], or in mini pigs with hypercholesterolemia[5].

In contrast, the way in which CAV correlates with coronary capillary density or coronary flow reserve is yet to be determined. As CAV measures the volume of arteries far larger than capillaries, these problems need to be resolved (eg, by animal experiments) before we can measure CAV in patients with a wide variety of cardiovascular diseases.

It is also reasonable to assume CAV may provide information other than coronary capillary density or coronary flow reserve. In Ehara et al, CAV is only measured under nitroglycerine. The response of CAV to increased coronary flow or to endothelium-dependent vasodilatation may be of clinical value. If better accuracy and reproducibility is established, CAV may potentially replace quantitative coronary angiography for this purpose because of its noninvasive nature.

Is CAV Really Unmatched With LVM?

The authors' conclusion of unmatched CAV with LVM should be discussed. **Figure** shows the linear regression between CAV and LVM reproduced and modified from Figure 6 of Ehara et al. The modified figure has extended axes and the extrapolated regression line has been added.

Even though there is only a single data set for each patient, the authors assumed that the line started at the origin and calculated the slope. Schematically, they have compared the slopes of dashed lines.

Figure, however, indicates that the CAV–LVM relationship obtained from pooled data has a positive CAV offset, but does note indicate that the slope is shallow. Because there is no reason to deny the presence of a positive CAV offset, and because the slope was not compared with a standard slope, the conclusion of unmatched CAV with LVM is not solid.

This question may be resolved by comparing the CAV–LVM relationship obtained by sequential CAV measurement during physiological growth and that obtained during the progression of pathological hypertrophy of the heart in animal experiments.

Advantage of CAV Measurement

The noninvasive nature of CAV measurement enhances its clinical usefulness because it enables sequential evaluation and may help to bring evaluations still in the investigational stage into routine bedside practice. Similar technological developments (eg, coronary flow reserve by cine magnetic resonance[6]) may be combined and eventually enable the detailed pathophysiology of cardiovascular disease to be described.

References

1. Ehara S, Okuyama T, Shirai N, Sugioka K, Oe H, Itoh T, et al. Inadequate increase in the volume of major epicardial coronary arteries compared with that in left ventricular mass: Novel concept for characterization of coronary arteries using 64-slice computed tomography. *Circ J* 2009; **73:** 1448–1453.
2. Tomanek RJ, Wessel TJ, Harrison DG. Capillary growth and geometry during long-term hypertension and myocardial hypertrophy in dogs. *Am J Physiol* 1991; **261:** H1011–H1018.
3. Krams R, Kofflard MJ, Duncker DJ, Von Birgelen C, Carlier S, Kliffen M, et al. Decreased coronary flow reserve in hypertrophic cardiomyopathy is related to remodeling of the coronary microcirculation. *Circulation* 1998; **97:** 230–233.
4. Tsagalou EP, Anastasiou-Nana M, Agapitos E, Gika A, Drakos SG, Terrovitis JV, et al. Depressed coronary flow reserve is associated with decreased myocardial capillary density in patients with heart failure due to idiopathic dilated cardiomyopathy. *J Am Coll Cardiol* 2008; **52:** 1391–1398.
5. Theilmeier G, Verhamme P, Dymarkowski S, Beck H, Bernar H, Lox M, et al. Hypercholesterolemia in minipigs impairs left ventricular response to stress: Association with decreased coronary flow reserve and reduced capillary density. *Circulation* 2002; **106:** 1140–1146.
6. Sakuma H, Koskenvuo JW, Niemi P, Kawada N, Toikka JO, Knuuti J, et al. Assessment of coronary flow reserve using fast velocity-encoded cine MR imaging: Validation study using positron emission tomography. *Am J Roentgenol* 2000; **175:** 1029–1033.

31st Annual International Conference of the IEEE EMBS
Minneapolis, Minnesota, USA, September 2-6, 2009

Feedback Control of Multiple Hemodynamic Variables with Multiple Cardiovascular Drugs

Masaru Sugimachi, *Member, IEEE*, Kazunori Uemura,
Atsunori Kamiya, Shuji Shimizu, Masashi Inagaki, and Toshiaki Shishido

Abstract— **The ultimate goal of disease treatment is to control the biological system beyond the native regulation to combat pathological process. To maximize the advantage of drugs, we attempted to pharmacologically control the biological system at will, e.g., control multiple hemodynamic variables with multiple cardiovascular drugs. A comprehensive physiological cardiovascular model enabled us to evaluate cardiovascular properties (pump function, vascular resistance, and blood volume) and the feedback control of these properties. In 12 dogs, with dobutamine (5±3 $\mu g \cdot kg^{-1} \cdot min^{-1}$), nitroprusside (4±2 $\mu g \cdot kg^{-1} \cdot min^{-1}$), dextran (2±2 $ml \cdot kg^{-1}$), and furosemide (10 mg in one, 20 mg in one), rapid, sufficient and stable control of pump function, vascular resistance and blood volume resulted in similarly quick and stable control of blood pressure, cardiac output and left atrial pressure in 5±7, 7±5, and 12±10 minutes, respectively. These variables remained stable for 60 minutes (RMS 4±3 mmHg, 5±2 $ml \cdot min^{-1} \cdot kg^{-1}$, 0.8±0.6 mmHg, respectively).**

I. Introduction

THE ultimate goal of disease treatment is to control the biological system beyond the native regulation to combat pathological process. This control may be partly achieved by native regulatory systems, but these frequently fail when disease progresses.

Many pharmacological treatments have provided us with control measures that may act in ways not possible by native regulators. To fully take advantage of these medicines, we must establish ways of using these agents to control the biological system at our will. As an example, we tried to control multiple hemodynamic variables with multiple cardiovascular drugs.

Several closed-loop systems have succeeded in directly controlling a single hemodynamic variable [1,2]. Multiple-variable control, however, has been unsuccessful [3-5].

Multiple-input multiple-output feedback control remains a challenge if the input-output relationships for all combinations are of equal significance. We therefore tried to decouple the input-output relationships by using a comprehensive physiological cardiovascular model. The model enabled us to define a set of parallel independent relationships between cardiovascular properties and drugs: pump function / inotrope, vascular resistance / vasodilator, and blood volume / volume expander. The model also provided us with a method to quantitatively calculate cardiovascular properties.

Manuscript received April 7, 2009. This work was supported in part by Grant-in-Aid for Scientific Research (B 20300164, C 20500404) from the Ministry of Education, Culture, Sports, Science and Technology, by Health and Labour Sciences Research Grants (H19-nano-ippan-009, H20-katsudo -shitei-007) from the Ministry of Health, Labour and Welfare of Japan.

M. Sugimachi, K. Uemura, A. Kamiya, S. Shimizu, M. Inagaki, and T. Shishido are with the National Cardiovascular Center Research Institute, Suita, Osaka 5658565, Japan (corresponding author Masaru Sugimachi to provide phone: +81-6-6833-512; fax: +81-6-6835-5403; e-mail: su91mach@ri.ncvc.go.jp).

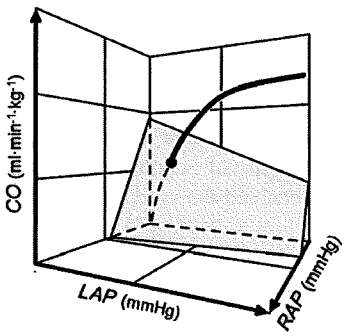

Fig. 1. Extended Guyton's model.
Thick curve, pump function of left and right heart; shaded surface, capacitive function of total vascular beds; CO, cardiac output; LAP, left atrial pressure; RAP, right atrial pressure.

II. Model and Methods

A. Cardiovascular property identification

Abnormalities of hemodynamic variables arise from abnormalities of cardiovascular properties, including pump function, vascular resistance, and blood volume. We identified these properties using an extended version of Guyton's circulatory equilibrium framework (Fig. 1) [6,7].

Pump function of the left heart (S_L) can be quantified as the ratio of cardiac output (CO) to the logarithm of left atrial pressure (LAP) ($S_L = CO / [\ln (LAP - 2.03) + 0.80]$). Systemic vascular resistance (R) can be calculated as blood pressure (BP) minus right atrial pressure (RAP) divided by CO. Stressed total blood volume (V) is obtained by $V = (CO + 19.61\ RAP + 3.49\ LAP) \times 0.129$.

B. Autopilot System

Autopilot controller of multiple hemodynamic variables consisted of multiple feedback loops. We designed these

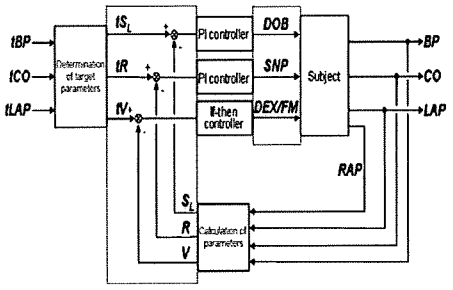

Fig. 2. Autopilot controller.
Calculated cardiovascular properties, rather than hemodynamic variables, were feedback-controlled to achieve multiple independent control of variables.

feedbacks as being independent of each other. The selection and the combination of controlled property and the controlling drugs enabled the independent operation (Fig. 2) [8].

S_L and R were controlled by proportional-integral (PI) feedback, with infusion of dobutamine (DOB) and sodium nitroprusside (SNP), respectively. Proportional and integral gain values were calculated using Chien-Hrones-Reswick's method [9] from gain, time constant, and dead-time delay of the approximated first-order step responses of S_L to DOB and R to SNP. We infused 10% dextran 40 solution (DEX, 10 $ml \cdot min^{-1}$) as long as V was <1 $ml \cdot kg^{-1}$ than the target, and injected furosemide (FM, 10 mg) every 20 minutes while V was >2 $ml \cdot kg^{-1}$ than the target.

C. *Animal Experiments*

We evaluated the performance of the autopilot controller in 12 adult anesthetized mongrel dogs (both sexes, 25±4 kg). We measured BP, CO, LAP and RAP. DOB, SNP, and DEX were automatically administered into the femoral vein through independent infusion routes, using either a computer-controlled roller pump or an infusion pump. FM was given through the jugular vein manually according to computer instructions.

These dogs underwent coronary microembolization, resulting in left ventricular failure. After hemodynamic stabilization, we began implementing control using the autopilot system.

III. Results

	Proportional gain (K_p) $\mu g \cdot ml^{-1}$	Integral gain (K_i) sec^{-1}
S_L control	0.06	0.01
R control	-1.37	0.007

Table 1. Selected gain parameters for designed controller.
Dose ($\mu g \cdot kg^{-1} \cdot min^{-1}$) of drugs for the control of S_L (DOB) or R (SNP) is determined as (Dose) = $K_p(1 + K_i / s)\,\Delta$(Controlled variable)

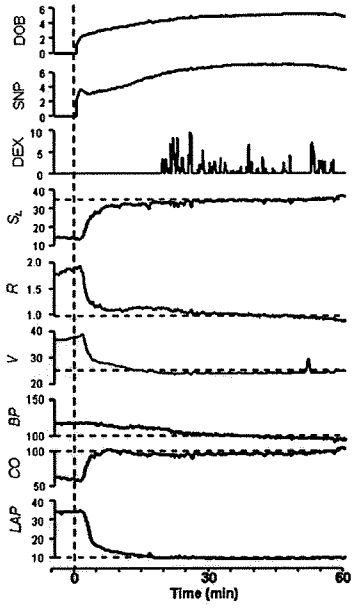

Fig. 3. An example of the automatic control of hemodynamics.
Feedback control was rapid, sufficient, and stable. DOB, dobutamine ($\mu g \cdot kg^{-1} \cdot min^{-1}$); SNP, sodium nitroprusside ($\mu g \cdot kg^{-1} \cdot min^{-1}$); DEX, dextran 40 solution ($ml \cdot min^{-1}$); S_L, pump function ($ml \cdot kg^{-1} \cdot min^{-1}$); R, resistance ($mmHg \cdot ml^{-1} \cdot kg \cdot min$); V, blood volume ($ml \cdot kg^{-1}$); BP, blood pressure (mmHg); CO, cardiac output ($ml \cdot kg^{-1} \cdot min^{-1}$); LAP, left atrial pressure (mmHg)

Based on the step response from coronary microembolized dogs, we determined the proportional and integral gain as shown in Table 1.

Similar to the example shown in Figure 3, in 12 dogs, by administering DOB (5±3 $\mu g \cdot kg^{-1} \cdot min^{-1}$), SNP (4±2 $\mu g \cdot kg^{-1} \cdot min^{-1}$), DEX (2±2 $ml \cdot kg^{-1}$), and FM (10 mg in one, 20 mg in one), rapid, sufficient and stable control of S_L, R and V. This resulted in corresponding appropriate control of BP, CO and LAP in 5±7, 7±5, and 12±10 minutes, respectively. These remained stable for 60 minutes (RMS BP=4±3 mmHg, CO=5±2 $ml \cdot min^{-1} \cdot kg^{-1}$, LAP=0.8±0.6 mmHg).

IV. Discussion

We have shown that by evaluating cardiovascular properties (pump function, vascular resistance, and blood volume), and then controlling these properties with individually selected drugs, we were able to automatically control multiple hemodynamic abnormalities rapidly, stably, and simultaneously.

Direct control of multiple hemodynamic variables, however, likely fails because each drug affects more than one variable. Direct control remains unfeasible even with more complicated methods developed in control engineering; appropriate physiological modeling and precise evaluation of cardiovascular properties are essential to achieving adequate control.

V. CONCLUSION

Calculating cardiovascular properties (pump function, vascular resistance, and blood volume) based on a comprehensive cardiovascular model and feedback control of these properties are required for the accurate control of multiple hemodynamic variables (BP, CO, LAP).

REFERENCES

[1] W. R. Chitwood, Jr, D. M. Cosgrove III, R. M. Lust, "Multicenter trial of automated nitroprusside infusion for postoperative hypertension. Titrator Multicenter Study Group," *Ann. Thorac. Surg.* Vol. 54, 517–522, 1992.

[2] D. M. Cosgrove III, J. H. Petre, J. L. Waller, J. V. Roth, C. Shepherd, *et al*, "Automated control of postoperative hypertension: a prospective, randomized multicenter study," *Ann. Thorac. Surg.* Vol. 47, 678–682, 1989.

[3] S. A. Hoeksel, J. A. Blom, J. R. Jansen, J. G. Maessen, J. J. Schreuder, "Automated infusion of vasoactive and inotropic drugs to control arterial and pulmonary pressures during cardiac surgery," *Crit. Care Med.* Vol. 27, 2792–2798, 1999.

[4] G. I. Voss, P. G. Katona, H. J. Chizeck, "Adaptive multivariable drug delivery: control of arterial pressure and cardiac output in anesthetized dogs," *IEEE Trans. Biomed. Eng.* Vol. 34, 617–623, 1987.

[5] C. Yu, R. J. Roy, H. Kaufman, B. W. Bequette, "Multiple-model adaptive predictive control of mean arterial pressure and cardiac output," *IEEE Trans. Biomed. Eng.* Vol. 39, 765–778, 1992.

[6] K. Uemura, M. Sugimachi, T. Kawada, A. Kamiya, Y. Jin, *et al.*, "A novel framework of circulatory equilibrium," *Am. J. Physiol. Heart Circ. Physiol.* vol. 286, no. 6, pp. H2376–H2385, Jun. 2004.

[7] K. Uemura, T. Kawada, A. Kamiya, T. Aiba, I. Hidaka, *et al.*, "Prediction of circulatory equilibrium in response to changes in stressed blood volume," *Am. J. Physiol. Heart Circ. Physiol.* vol. 289, no. 1, H301–H307, Jul. 2005.

[8] K. Uemura, A. Kamiya, I. Hidaka, T. Kawada, S. Shimizu, *et al.*, "Automated drug delivery system to control systemic arterial pressure, cardiac output, and left heart filling pressure in acute decompensated heart failure," *J. Appl. Physiol.* vol. 100, no. 4, 1278–1286, Apr. 2006.

[9] K. L. Chien, J. A. Hrones, J. B. Reswick, "On the automatic control of generalized passive systems," *Trans. ASME.* Vol. 74, 175–185, 1952.

31st Annual International Conference of the IEEE EMBS
Minneapolis, Minnesota, USA, September 2-6, 2009

Macroscopic Two-Pump Two-Vasculature Cardiovascular Model to Support Treatment of Acute Heart Failure

Masaru Sugimachi, *Member, IEEE*, Kenji Sunagawa, *Member, IEEE*,
Kazunori Uemura, Atsunori Kamiya, Shuji Shimizu, Masashi Inagaki and Toshiaki Shishido

Abstract— **Comprehensive understanding of hemodynamics remains a challenge even for expert cardiologists, partially due to a lack of an appropriate macroscopic model. We attempted to amend three major problems of Guyton's conceptual model (unknown left atrial pressure, unilateral heart damage, blood redistribution) and developed a comprehensive macroscopic model of hemodynamics that provides quantitative information. We incorporated a third axis of left atrial pressure, resulting in a 3D coordinate system. Pump functions of left and right heart are expressed by an integrated cardiac output curve, and the capacitive function of total vasculature by a venous return surface. The equations for both the cardiac output curve and venous return surface would facilitate precise diagnosis (especially evaluation of blood volume) and choice of appropriate treatments, including application to autopilot systems.**

I. Introduction

COMPREHSNSIVE understanding of hemodynamics remains a challenge even for specialist clinicians including cardiologists. This is in part attributed to a lack of an appropriate macroscopic model of hemodynamics that would facilitate reasoning. Most cardiologists relied only on, if at all, the classical Guyton's circulatory equilibrium framework [1].

Guyton's model consists of only two subdivisions of the whole circulation: the cardiopulmonary component (in which both hearts and pulmonary vasculature are lumped) and the systemic vascular bed. These two subdivisions are characterized by the 'cardiac output curve' and 'venous return curve', respectively. The 'cardiac output curve' approximated the (total) pump function, and the 'venous return curve' approximated the capacitive function of systemic vasculature. The intersection of these curves coincides with the operating point of the circulation.

Guyton's model is, however, inappropriate (see MODEL AND METHODS) for the understanding of hemodynamics in patients with, for example, acute myocardial infarction, where only one ventricle is preferentially damaged. That is why many cardiologists gradually abandoned using Guyton's model for their reasoning.

If we can amend the shortcomings of Guyton's model and develop a more appropriate model, the new model would obviously help diagnosis procedures and treatment selection. Furthermore, the model may be able to quantify the hemodynamic abnormalities rather than just to identify them.

Therefore, the aim of this study was to develop a comprehensive macroscopic model of hemodynamics that would provide quantitative information and aid diagnosis and treatments.

Manuscript received April 7, 2009. This work was supported in part by Grant-in-Aid for Scientific Research (B 20300164, C 20500404) from the Ministry of Education, Culture, Sports, Science and Technology, by Health and Labour Sciences Research Grants (H19-nano-ippan-009, H20-katsudo -shitei-007) from the Ministry of Health Labour and Welfare of Japan.

M. Sugimachi, K. Uemura, A. Kamiya, S. Shimizu, M. Inagaki and T. Shishido are with the National Cardiovascular Center Research Institute, Suita, Osaka 5658565, Japan (corresponding author Masaru Sugimachi to provide phone: +81-6-6833-512; fax: +81-6-6835-5403; e-mail: su91mach@ri.ncvc.go.jp).

K. Sunagawa is with Kyushu University, Fukuoka 8128582 Japan. (e-mail: sunagawa@cardiol.med.kyushu-u.ac.jp).

II. Model and Methods

A. Shortcomings of Guyton's Model

Guyton's model has a number of problems when used in patients with unilateral heart failure.

First, the model does not provide left atrial pressure (LAP) values directly. LAP indicates the degree of pulmonary congestion and blood desaturation, and is as important as cardiac output (CO) and blood pressure.

Second, it is impossible to precisely model unilateral heart failure, which is frequently seen in patients with ischemic heart disease.

Third, in unilateral heart failure, the relative blood volumes in pulmonary and systemic vascular beds vary. As Guyton's model assumes only blood volume within the systemic vascular bed, such redistribution would shift the venous return curve even though the total blood volume remains the same.

B. Development of Comprehensive Cardiovascular Model

To solve the above problems, we extended Guyton's model.

First, a third axis of LAP was introduced in our new model (Fig. 1) [2], [3], so that LAP can be obtained directly. The pumping ability of the heart and the capacitive function of the vasculature are expressed simultaneously in the 3D space (RAP-LAP-CO coordinate system).

Second, the pumping abilities of the left and right heart are expressed separately by the respective cardiac output surfaces that are independent of each other. In an equilibrium state, by matching the cardiac output of both sides, the pumping ability of the whole heart can be integrated and expressed by a curve

expressing the intersection of the two surfaces (integrated cardiac output curve, Fig. 1, thick curve).

Third, the capacitive function of total vasculature (including both systemic and pulmonary vasculatures) is expressed by the venous return surface (Fig. 1, shaded surface), which is an extension of the venous return curve. This surface expresses the changes in LAP and right atrial pressure (RAP) in response to CO change, while the total intravascular blood volume remains constant. In addition, blood redistribution between systemic and pulmonary vasculatures (without change in total blood volume) will be expressed by movement within the surface rather than by deviation from the surface.

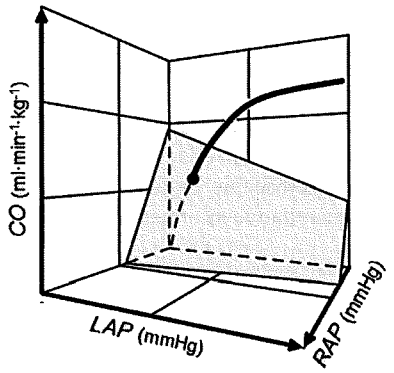

Fig. 1. An original macroscopic model of hemodynamics (an extended Guyton's model). The curve expresses the integrated pumping ability of left and right heart. The shaded surface characterizes the capacitive function of the total (systemic + pulmonary) vasculatures. The surface remains constant as long as the total intravascular blood volume remains the same. CO, cardiac output; LAP, left atrial pressure; RAP, right atrial pressure.

C. Animal Experiments to Characterize Venous Return Surface

Figure 2 depicts the scheme of an experiment to characterize the venous return surface. We replaced the left and right heart with roller pumps, which allows us to change CO of the right heart or left heart independently.

By adjusting the flow (i.e., CO) of the two pumps to the same level, the changes in RAP and LAP in response to a change in CO can be observed. Blood redistribution between systemic and pulmonary vasculatures can be reproduced by transiently unbalancing the flow of the two pumps.

From each dog (n = 6), we obtained 6 different sets of data (CO, RAP, LAP). These data were subjected to bivariate linear regression using RAP and LAP as independent variables and CO as the dependent variable.

III. Results

Figure 3 illustrates the venous return surfaces obtained from 6 dogs. Bivariate linear regression in each animal yielded a flat surface in 3D space. The surface is shown as a line in Fig. 3, because we have projected the surface in a

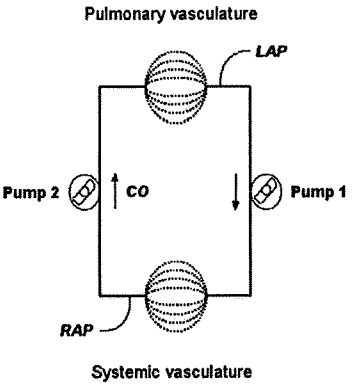

Fig. 2. An experimental scheme to characterize venous return surface. By replacing the left and right heart with roller pumps, one can change cardiac output of the right heart or left heart independently.

direction parallel to the surface. The experimental data obtained from each of the 6 animals showed good fit with the surface. In addition, the surfaces obtained from 6 animals were almost parallel, as shown by the nearly parallel 3D coordinate axes. These experimental results indicated that the venous return surface is linear and can be expressed by a common equation for all animals.

Further, by infusing or withdrawing known amounts of blood, we were able to derive an equation for the venous return surface as follows:

$$CO = V / 0.129 - 19.61\ RAP - 3.49\ LAP$$

where V is total intravascular stressed blood volume. This formula [$V = (CO + 19.61\ RAP + 3.49\ LAP) \times 0.129$] can be used to quantify V from CO, RAP and LAP.

We also succeeded to quantify the integrated cardiac output curve by logarithmic functions as follows:

$$CO = S_L\ [\ln(LAP-2.03)+0.80]$$

$$CO = S_R\ [\ln(RAP-2.13)+1.90]$$

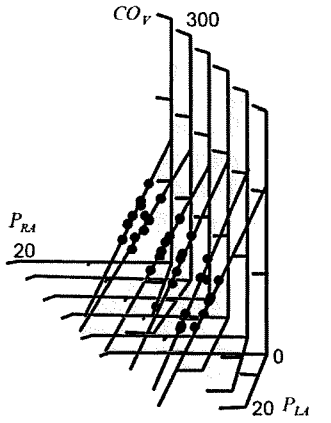

Fig. 3. Superimposed venous return surfaces obtained from 6 dogs. For each dog, the venous return surface (RAP-LAP-CO relationship) in 3D coordinate system was projected in a direction parallel to the surface, and was superimposed with each other.

where S_L and S_R are parameters expressing the pumping ability of the left and right heart, respectively. These equations are also useful for quantifying the pumping ability of right and left heart (S_L = CO / [ln(LAP - 2.03) + 0.80], S_R = CO / [ln(RAP - 2.13) + 1.90]).

Using this model, we are able to predict with acceptable precision the hemodynamics after infusion or withdrawal of known amounts of blood (CO: $y = 0.93x + 6.5$, $r^2 = 0.96$, SEE = 7.5 ml·min^{-1}·kg^{-1}; LAP: $y = 0.90x + 0.5$, $r^2 = 0.93$, SEE = 1.4 mmHg; RAP: $y = 0.87x + 0.4$, $r^2 = 0.91$, SEE = 0.4 mmHg) (Fig. 4) [3].

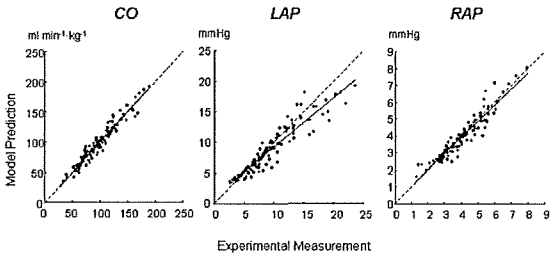

Fig. 4. Prediction of CO, LAP, and RAP based on our comprehensive macroscopic model of hemodynamics.

IV. Discussion

A. Difficulty in Decision Making of Heart Failure Treatment

Three hemodynamic variables: blood pressure, CO and LAP, appear to be the most essential factors influencing the survival of patients with heart failure. Our model clearly indicates that pump functions of left and right heart and total intravascular blood volume are determinants of CO and LAP. Systemic vascular resistance is an additional determinant of blood pressure.

For clinicians, the evaluation of blood volume is relatively difficult compared to pump functions and vascular resistance. In practice, clinicians have been using RAP as a proxy for blood volume. It is clear from our results [V = (CO + 19.61 RAP + 3.49 LAP) × 0.129] that blood volume (V) is not solely determined by RAP. Rather, all three parameters of CO, RAP and LAP are necessary to evaluate blood volume. The equation indicates that an increase of RAP by 1 mmHg is equivalent to an LAP increase of 5.6 mmHg, and a CO increase of 19.61 mL/min/kg (ca. 0.98 L/min for a 50-kg patient).

B. Application of the Model: Autopilot System

The biggest benefit of our comprehensive visual model of hemodynamics is that it enables us to diagnose the abnormality of cardiovascular system in a quantitative manner. This would lead to appropriate selection of drugs and their doses.

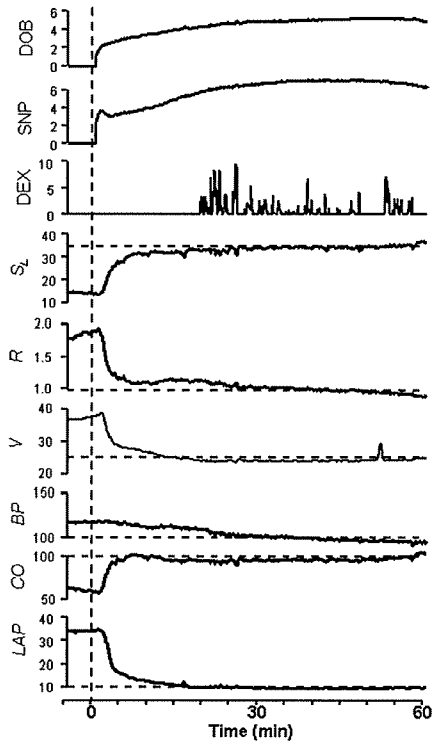

Fig. 5. An example of correction of hemodynamics with an autopilot system. By normalizing cardiovascular properties [pump function (S_L), resistance (R), blood volume (V)] with the administration of dobutamine (DOB), sodium nitroprusside (SNP), and dextran 40 solution (DEX), all the abnormal hemodynamic variables (increased blood pressure [BP], decreased cardiac output [CO], and elevated left atrial pressure [LAP]) were resolved rapidly, sufficiently, and stably.

As shown in Fig. 5, by translating hemodynamic variables into cardiovascular properties (pump function, vascular resistance, and blood volume), and by controlling each of these parameters with individual drug with preferential effect on the parameter, we are able to correct automatically all the parameters of blood pressure, CO and LAP rapidly, stably, and simultaneously.

Using an autopilot system to administer dobutamine (DOB at 5 ± 3 mg·kg^{-1}·min^{-1}), nitroprusside (SNP at 4 ± 2 mg·kg^{-1}·min^{-1}), dextran infusion (DEX at 2 ± 2 ml·kg^{-1}), and furosemide (10 mg in one, 20 mg in one) in 12 dogs with acute heart failure rapidly normalized blood pressure, CO, and LAP in 5 ± 7, 7 ± 5, and 12 ± 10 minutes, respectively. The normalized values remained stable thereafter (RMS values, blood pressure = 4 ± 3 mmHg, CO = 5 ± 2 ml·min^{-1}·kg^{-1}, LAP = 0.8 ± 0.6 mmHg).

V. Conclusion

We have successfully developed a comprehensive macroscopic model of hemodynamics that provides quantitative information. Using a 3D coordinate system, the pump functions of left and right heart are expressed by an

integrated cardiac output curve, and the capacitive function of total vasculature by a venous return surface. The equations of both the cardiac output curve and venous return surface would facilitate accurate diagnosis (especially evaluation of blood volume) and choice of appropriate treatments, including application to autopilot systems.

REFERENCES

[1] A. C. Guyton, "Determination of cardiac output by equating venous return curves with cardiac response curves," *Physiol. Rev.* vol. 35, no. 1,123–129, Jan. 1955.

[2] K. Uemura, M. Sugimachi, T. Kawada, A. Kamiya, Y. Jin, *et al.*, "A novel framework of circulatory equilibrium," *Am. J. Physiol. Heart Circ. Physiol.* vol. 286, no. 6, pp. H2376–H2385, Jun. 2004.

[3] K. Uemura, T. Kawada, A. Kamiya, T. Aiba, I. Hidaka, *et al.*, "Prediction of circulatory equilibrium in response to changes in stressed blood volume," *Am. J. Physiol. Heart Circ. Physiol.* vol. 289, no. 1, H301–H307, Jul. 2005.

Case Reports

Destructive Device Removal - Sparks and Deletion of Therapy History From an Implantable Cardioverter Defibrillator

Takashi KURITA,[1] MD, Shigeyuki UEDA,[2] MD, Hideo OKAMURA,[2] MD, Takashi NODA,[2] MD, Kazuhiro SATOMI,[2] MD, Kazuhiro SUYAMA,[2] MD, Wataru SHIMIZU,[2] MD, Naohiko AIHARA,[2] MD, Shunichi MIYAZAKI,[1] MD *and* Shiro KAMAKURA,[2] MD,

SUMMARY

A 74-year-old female with a diagnosis of idiopathic dilated cardiomyopathy and ventricular tachycardia died suddenly 9 years after an implantation of an implantable cardioverter-defibrillator (ICD). The destructive removal of an ICD generator and the leads by an uninformed coroner resulted in the loss of the fragile electrograms during the terminal episodes of VT/VF and caused severe charring on the surface of the ICD generator.

In order to observe the conditions in which the shock deliveries occurred during the noise detection, we programmed the ICD to deliver the maximum shock energy via a programmer while keeping continuous contact between the device surface and shock lead. The maximum shock energy of 31 Joules produced significant sparks from the surface of the ICD.

To avoid the loss of data from an ICD and injury to the patient, widespread notification and education through appropriate scientific societies about the functions of ICDs are highly recommended. (Int Heart J 2009; 50: 823-827)

Key words: Sudden cardiac death, Implantable device, Device removal

THIS case report describes the destructive removal of an ICD generator and the leads by an unaware person may result in the loss of important information, such as the electrograms during the terminal episodes of VT/VF, and may cause severe charring on the surface of the ICD generator. The publication of this case will hopefully contribute to avoiding the loss of data from an ICD and injury to the person.

Implantable cardioverter defibrillators (ICDs) are well established as the

From the [1] Division of Cardiology, Department of Internal Medicine, Kinki University School of Medicine and [2] Division of Cardiology, Department of Internal Medicine, National Cardiovascular Center, Osaka, Japan.

Address for correspondence: Takashi Kurita, MD, Division of Cardiology, Department of Internal Medicine, Kinki University School of Medicine, 377-2, Ohno-Higashi, Osaka-Sayama, Osaka 589-8511, Japan.

Received for publication May 8, 2009.

Revised and accepted August 6, 2009.

most effective antiarrhythmic therapy for patients with ventricular tachycardia (VT) and/or ventricular fibrillation (VF). However, several clinical studies[1-3] have demonstrated that the annual incidence of sudden death in patients with ICDs is presumed to be approximately 2%. Sudden death cannot be completely avoided even after ICD therapy.

The therapy logs and electrograms at the time of sudden death are very useful for evaluating the mode of death in such clinical settings. However, inappropriate manipulation of an ICD and the leads after death may result in the loss of important fragile information during a fatal event. Therefore, general physicians, police officers, and paramedics, who may encounter unexpected out-of-hospital deaths of ICD patients, should be informed about proper management of the device after the death of an ICD patient. In Japan, almost all deceased persons are cremated. Therefore, removal of the ICD generator is recommended before cremation in order to avoid explosion of the ICD generator under the high temperatures used in cremation. We experienced an out-of-hospital patient who died suddenly and her ICD was removed by a coroner who mistakenly left it in the active state.

Case report

The case was a 74 year-old female with a diagnosis of idiopathic dilated cardiomyopathy and ventricular tachycardia. An ICD was implanted on February 26, 1997. After implantation, she experienced 6 episodes of appropriate antitachycardia pacing or shock therapies during 9 years of follow-up. On January 26, 2007, her husband noted that she had gone to her bedroom at 14:30. At 18:00 pm, he discovered she had collapsed on her bed and showed no response to his calls. An emergency rescue team arrived 20 minutes later but she had already passed away.

A coroner's inquest was begun at 21:05 on the same day. Because it was the first time the coroner had performed an autopsy on a patient with an ICD, he removed the ICD by cutting the leads forcibly using scissors without inactivating the device beforehand. After extracting the ICD, he placed the generator in a plastic bag with the damaged leads attached, and kept it in his office.

We became aware of her sudden death one month later due to her absence from our out-patient clinic. We contacted the coroner through the police department and requested that he send the device to our hospital. To evaluate the cause of the sudden death, we retrieved data from the ICD using a programmer. Unfortunately, the electrograms during the fatal event were subsequently lost because of the repeated noise events sensed after removal of the device. The remaining log data were retrieved from the ICD. Four VT or VF events were detected

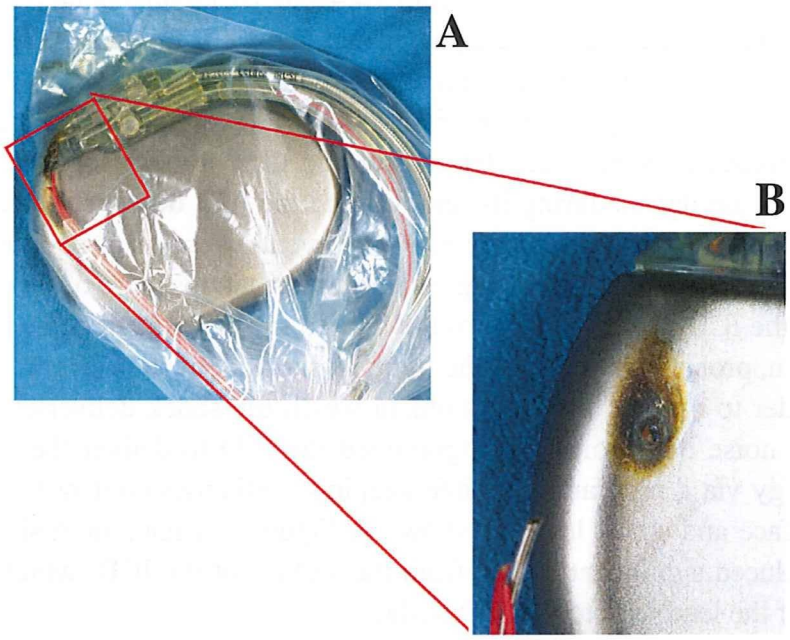

Figure 1. Charring and crater formation on the surface of the ICD.
A: The ICD had been placed in a vinyl bag with the damaged leads still attached.
B: A magnified view of the uncovered ICD surface. Significant craters and charring are observed where the edge of the damaged shock lead came in contact with the ICD can.

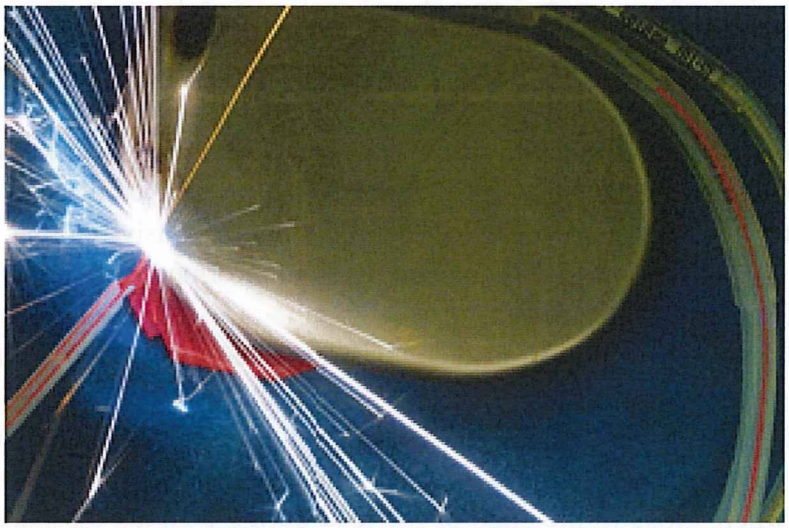

Figure 2. A maximum shock of 31 Joules produced significant sparks emanating from the surface of the ICD.

within approximately 20 minutes (from 14:49 to 15:11 on January 26, 2007), and ICD therapies (antitachycardia pacing and defibrillation shocks) in response to each episode were delivered. After the terminal shock therapy, back-up ventricular pacing with a cycle length of 1000 ms was present. From 21:21 on the same day, frequent events were detected during the coroner's inquest with manipulation of the device during its removal and the ICD delivered many shocks that were triggered by sensing noise. Many events were also recorded on the 26th and 28th of February. Charring and crater formations were observed on the surface of the ICD where the edge of the injured shock lead had come in contact with the can, probably because of the frequent shock deliveries (Figure 1).

In order to observe the conditions in which the shock deliveries occurred during the noise detection, we programmed the ICD to deliver the maximum shock energy via a programmer while keeping continuous contact between the device surface and shock lead. As shown in Figure 2, a maximum shock of 31 Joules produced significant sparks from the surface of the ICD, which resulted in fusion of the lead wire to the ICD surface.

Discussion

We report a patient with idiopathic dilated cardiomyopathy and a history of VT/VF in whom an ICD and the leads were destructively removed by an unaware coroner after the sudden cardiac death of the patient. Because the electrograms during the fatal event had disappeared due to successive detections of noise, the exact cause of the sudden death remained unknown. However, the remaining stored data logs and event markers (showing frequent VT/VF episodes followed by continuous back-up pacing) suggested that the terminal defibrillation shock was either unsuccessful in terminating the tachycardia due to degenerating it to fine (undetectable) VF or induced a nonresponsive cardiac electrical standstill. A postmortum ICD extraction by an uninformed person could lead to the loss of important information.

Furthermore, the present case demonstrated that unstable contact between the uncovered edge of a lead and the surface of the ICD may cause dangerous electric discharges. The melting point of titanium (the material on the surface of ICD generators) is reported to be approximately 1600 °C. If a person were to touch anywhere close to the edge of the lead during a shock discharge, it may cause severe injury.

Even in the United States where the deceased are usually buried, inactivation and removal of an ICD for analysis has been recommended by manufacturers.

To avoid both deletion of the therapy history and dangerous electrical dis-

charges from the ICD, the following procedures are recommended. 1) Careful disconnection of the lead from the ICD using a special screwdriver. 2) Inactivation of the device by changing the previous settings using a compatible programmer. 3) When a coroner or pathologist does not have special implements to perform the above procedures, he or she has no choice but to remove the device by cutting the ICD leads after placing insulation between the edges of the injured leads and the surface of the ICD in order to prevent electrical shock. 4) After removal of the device, the coroner or police department should inform the patient's doctor about the death as soon as possible. 5) The device should be sent to an appropriate medical center or the manufacturer so they can analyze the terminal episode. In order to ensure widespread and consistent notification about the handling of ICDs after death, education through appropriate scientific societies, such as a guideline from the Japanese Heart Rhythm Society, is highly recommended.

Acknowledgment

We would like to thank Mr. Hajime Ideno, Technical Service Manager, Boston Scientific, Guidant Japan, KK for his support in preparing Figure 2 which demonstrates significant sparks from an ICD.

References

1. Connolly SJ, Gent M, Roberts RS, *et al.* Canadian implantable defibrillator study (CIDS): A randomized trial of the implantable cardioverter defibrillator against amiodarone. Circulation 2000; 101: 1297-302.
2. Powell AC, Fuchs T, Finkelstein DM, *et al.* Influence of implantable cardioverter-defibrillators on the long-term prognosis of survivors of out-of-hospital cardiac arrest. Circulation 1993; 88: 1083-92.
3. A comparison of antiarrhythmic-drug therapy with implantable defibrillators in patients resuscitated from near-fatal ventricular arrhythmias. The Antiarrhythmics versus Implantable Defibrillators (AVID) Investigators. N Engl J Med 1997; 337: 1576-83.

Journal of the American College of Cardiology
© 2009 by the American College of Cardiology Foundation
Published by Elsevier Inc.

Vol. 54, No. 22, 2009
ISSN 0735-1097/09/$36.00
doi:10.1016/j.jacc.2009.08.028

QUARTERLY FOCUS ISSUE: HEART RHYTHM DISORDERS

Genotype-Phenotype Aspects of Type 2 Long QT Syndrome

Wataru Shimizu, MD, PHD,* Arthur J. Moss, MD,‡ Arthur A. M. Wilde, MD, PHD,‖ Jeffrey A. Towbin, MD,# Michael J. Ackerman, MD, PHD,** Craig T. January, MD, PHD,†† David J. Tester, BS,** Wojciech Zareba, MD, PHD,‡ Jennifer L. Robinson, MS,‡ Ming Qi, PHD,§ G. Michael Vincent, MD,‡‡ Elizabeth S. Kaufman, MD,§§ Nynke Hofman, MSC,¶ Takashi Noda, MD, PHD,* Shiro Kamakura, MD, PHD,* Yoshihiro Miyamoto, MD, PHD,† Samit Shah, BA,‡ Vinit Amin, MA,‡ Ilan Goldenberg, MD,‡ Mark L. Andrews, BBA,‡ Scott McNitt, MS‡

Osaka, Japan; Rochester, New York; Amsterdam, the Netherlands; Houston, Texas; Rochester, Minnesota; Madison, Wisconsin; Salt Lake City, Utah; and Cleveland, Ohio

Objectives The purpose of this study was to investigate the effect of location, coding type, and topology of *KCNH2(hERG)* mutations on clinical phenotype in type 2 long QT syndrome (LQTS).

Background Previous studies were limited by population size in their ability to examine phenotypic effect of location, type, and topology.

Methods Study subjects included 858 type 2 LQTS patients with 162 different *KCNH2* mutations in 213 proband-identified families. The Cox proportional-hazards survivorship model was used to evaluate independent contributions of clinical and genetic factors to the first cardiac events.

Results For patients with missense mutations, the transmembrane pore (S5-loop-S6) and N-terminus regions were a significantly greater risk than the C-terminus region (hazard ratio [HR]: 2.87 and 1.86, respectively), but the transmembrane nonpore (S1–S4) region was not (HR: 1.19). Additionally, the transmembrane pore region was significantly riskier than the N-terminus or transmembrane nonpore regions (HR: 1.54 and 2.42, respectively). However, for nonmissense mutations, these other regions were no longer riskier than the C-terminus (HR: 1.13, 0.77, and 0.46, respectively). Likewise, subjects with nonmissense mutations were at significantly higher risk than were subjects with missense mutations in the C-terminus region (HR: 2.00), but that was not the case in other regions. This mutation location–type interaction was significant ($p = 0.008$). A significantly higher risk was found in subjects with mutations located in α-helical domains than in subjects with mutations in β-sheet domains or other locations (HR: 1.74 and 1.33, respectively). Time-dependent β-blocker use was associated with a significant 63% reduction in the risk of first cardiac events ($p < 0.001$).

Conclusions The *KCNH2* missense mutations located in the transmembrane S5-loop-S6 region are associated with the greatest risk. (J Am Coll Cardiol 2009;54:2052–62) © 2009 by the American College of Cardiology Foundation

From the *Division of Cardiology, Department of Internal Medicine, and †Laboratory of Molecular Genetics, National Cardiovascular Center, Suita, Osaka, Japan; ‡Cardiology Division, Department of Medicine, and the §Department of Pathology, University of Rochester School of Medicine and Dentistry, Rochester, New York; Departments of ‖Cardiology and ¶Clinical Genetics, Academic Medical Center, Amsterdam, the Netherlands; #Department of Pediatrics, Baylor College of Medicine, Texas Children's Hospital, Houston, Texas; **Departments of Medicine, Pediatrics, and Molecular Pharmacology, Mayo Clinic College of Medicine, Rochester, Minnesota; ††Departments of Medicine and Physiology, University of Wisconsin-Madison, Madison, Wisconsin; ‡‡University of Utah, School of Medicine, Salt Lake City, Utah; and the §§Heart and Vascular Research Center, MetroHealth Campus of Case Western Reserve University, Cleveland, Ohio. Dr. Ackerman has a consulting relationship and license agreement/royalty arrangement with PGxHealth (FAMILION). This work was supported in part by a Health Sciences Research Grant (H18-Research on Human Genome-002) and a Research Grant for the Cardiovascular Diseases (21C-8) from the Ministry of Health, Labour and Welfare, Japan (to Dr. Shimizu); research grants HL-33843 and HL-51618 (to Dr. Moss) and HL-60723 (to Dr. January) from the National Institutes of Health, Bethesda, Maryland; and grant 2000.059 from the Nederlandse Hartstichting, Amsterdam, the Netherlands (to Dr. Wilde). Dr. Ackerman has received support from Medtronic, PGxHealth, and Pfizer. Dr. January has received support from Cellular Dynamics International. Dr. Tester receives modest royalties from PGxHealth. Dr. Kaufman receives research support from CardioDx and St. Jude Medical. Drs. Shimizu, Moss, Wilde, Towbin, Ackerman, and January contributed equally to the original concept of this investigation.

Manuscript received May 31, 2009; revised manuscript received August 14, 2009, accepted August 24, 2009.

Long QT syndrome (LQTS) is a congenital disorder caused by mutations of several cardiac ion channel genes and is diagnosed clinically by a prolonged QT interval on the electrocardiogram (ECG) and variable clinical outcomes including arrhythmia-related syncope and sudden death (1,2). Mutations involving the *KCNH2* gene *(hERG* [human ether-a-go-go-related gene]), which codes for the pore-forming α-subunit of a cardiac K^+ channel, have been linked to the type 2 LQTS, the second most common variant of LQTS (3). The *KCNH2* mutations lead to a reduction in the rapid component of the delayed rectifier repolarizing current (I_{Kr}), which contributes to lengthening of the QT interval (4). The *KCNH2* subunits oligomerize to form a tetramer that inserts into the cell membrane to form the functional K^+ channel. Each subunit comprises 6 α-helical transmembrane segments (S1 to S6), where the K^+-selective pore is found between S5 and S6. The transmembrane segments are flanked by amino (N)- and carboxyl (C)-terminus regions (5–8). In a previous study of patients with type 2 LQTS, mutations in the pore region were associated with an increased risk for arrhythmia-related cardiac events when compared with patients with nonpore mutations (9). However, this study was limited by population size in its ability to examine the phenotypic effect of mutations within distinct domains of the nonpore region.

See page 2063

There are several coding types of mutations in genes that form the functional K^+ channel: missense, nonsense, splice site, in-frame deletion, and frameshift mutations (10). Missense mutations are point mutations that result in a single amino acid change within the protein; nonsense mutations generate a stop codon and can truncate the protein. Insertion and deletion mutations cause in-frame or frameshift mutations, the latter of which change the grouping of nucleotide bases into codons. Splice site mutations may alter splicing of messenger ribonucleic acid. In our recent cohort of type 1 LQTS (11), a missense mutation accounted for 81% of all the mutations, and the type of mutation (missense vs. nonmissense) was not an independent risk factor. On the other hand, nonmissense mutations such as frameshift and nonsense mutations have been reported to be more frequently identified in the type 2 LQTS patients (11,12).

Moreover, topology of mutations (α-helical domain, β-sheet domain, and other uncategorized location) has been recently reported to relate to the function of mutated channel in the type 2 LQTS patients (8).

We hypothesized that the distinct location, coding type, and topology of the channel mutation would have important influence on the phenotypic manifestations and clinical course of patients with type 2 LQTS. To test this hypothesis, we investigated the clinical aspects of 858 subjects having a spectrum of *KCNH2* mutations categorized by the distinct location, coding type, and topology of the channel mutations.

Abbreviations and Acronyms

ECG = electrocardiogram
I_{Kr} = rapid component of the delayed rectifier repolarizing current
LQTS = long QT syndrome
NMD = nonsense-mediated decay
QTc = corrected QT

Methods

Study population. The study population of 858 subjects was derived from 213 proband-identified families with genetically confirmed *KCNH2* mutations. The proband in each family had corrected QT (QTc) prolongation not due to a known cause. The subjects were drawn from the U.S. portion of the International LQTS (Rochester) Registry (n = 456), the Netherlands' (Amsterdam) LQTS Registry (n = 214), the Japanese (National Cardiovascular Center) LQTS Registry (n = 95), and the Mayo Clinic LQTS Registry (n = 93). All subjects or their guardians provided informed consent for the genetic and clinical studies. Not included in the study population were 58 subjects with evidence of 2 or more LQTS mutations and an additional 18 who had polymorphisms (p.R176W or p.R1047L) that the authors felt might reduce I_{Kr} current. A total of 201 of the 456 patients enrolled from the U.S. portion of the International LQTS Registry and 61 of the 95 patients from the Japanese LQTS Registry were reported in our prior reports (9,12).

Phenotype characterization. Routine clinical and electrocardiographic parameters were acquired at the time of enrollment in each of the registries. Follow-up was censored at age 41 years to minimize the influence of coronary disease on cardiac events. Measured parameters on the first recorded ECG included QT and R-R intervals in milliseconds, with QT corrected for heart rate by Bazett's formula. The QTc interval was expressed in its continuous form and categorized into 4 levels: <460, 460 to 499, 500 to 530, and >530 ms. The QTc interval was categorized into 3 levels: <500, 500 to 530, and >530 ms for the end point of lethal cardiac events (aborted cardiac arrest or LQTS-related sudden cardiac death), because there were few lethal cardiac events in the lowest QTc group (<460 ms). Clinical data were collected on prospectively designed forms with information on demographic characteristics, personal and family medical history, electrocardiographic findings, therapy, and end points during long-term follow-up. Data common to all 4 LQTS registries involving genetically identified patients with type 2 LQTS genotype were electronically merged into a common database for this study.

Genotype characterization. The *KCNH2* mutations were identified using standard genetic tests performed in molecular-genetic laboratories in the participating academic centers. From the Rochester registry, 60 subjects died of sudden cardiac death at a young age and were not genotyped. These 60 subjects were assumed to have the same

KCNH2 mutation as other affected close members of their respective family.

Genetic alterations of the amino acid sequence were characterized by location in the channel protein, by the type of mutation (missense, splice site, in-frame insertions/deletions, nonsense [stop codon], and frameshift), and by the topology of mutation (α-helical domain, β-sheet domain, and other uncategorized location) (Fig. 1). The transmembrane region of the *KCNH2* encoded channel was defined as the coding sequence involving amino acid residues from 398 through 657 (S5-loop-S6 region: 552 to 657), with the N-terminus region defined before residue 398, and the C-terminus region after residue 657 (Fig. 1) (13,14).

We evaluated the risk associated with 4 main prespecified regions: 1) N-terminus; 2) transmembrane "nonpore" region (S1–S4); 3) transmembrane "pore" region (S5-loop-S6); and 4) C-terminus. We also evaluated the risk associated with distinct types of mutation and topology of mutation.

Statistical analysis. Differences in the univariate characteristics by specific groupings were evaluated by standard statistical methods. The primary end point was time to syncope, aborted cardiac arrest, or sudden death, whichever occurred first. The cumulative probability of a first cardiac event was assessed by the Kaplan-Meier method, with significance testing by the log-rank statistic. The Cox proportional-hazards survivorship model was used to evaluate the independent contribution of clinical and genetic factors to the first occurrence of time-dependent cardiac events from birth through age 40 years (15). The Cox regression models, stratified by decade of birth year and allowing for time-dependent covariates, were fit to estimate the adjusted hazard ratio (HR) of each factor as a predictor of first cardiac events. We observed that sex was not proportional as a function of age, with crossover in risk at age 13 on univariate Kaplan-Meier analysis. To fulfill the assumption of proportional hazards for sex over the entire age range, a time-dependent covariate for sex (via an interaction with time) was incorporated, allowing for different hazard ratios by sex before and after age 13 years.

Since almost all subjects were first- and second-degree relatives of probands, the effect of potential lack of independence between subjects was evaluated by refitting the Cox model using the robust sandwich estimator for family membership (16). All significant predictors of risk maintained significance using this robust measure of variance.

Patients who did not have an ECG for QTc measurement were identified in the Cox models as "QTc missing."

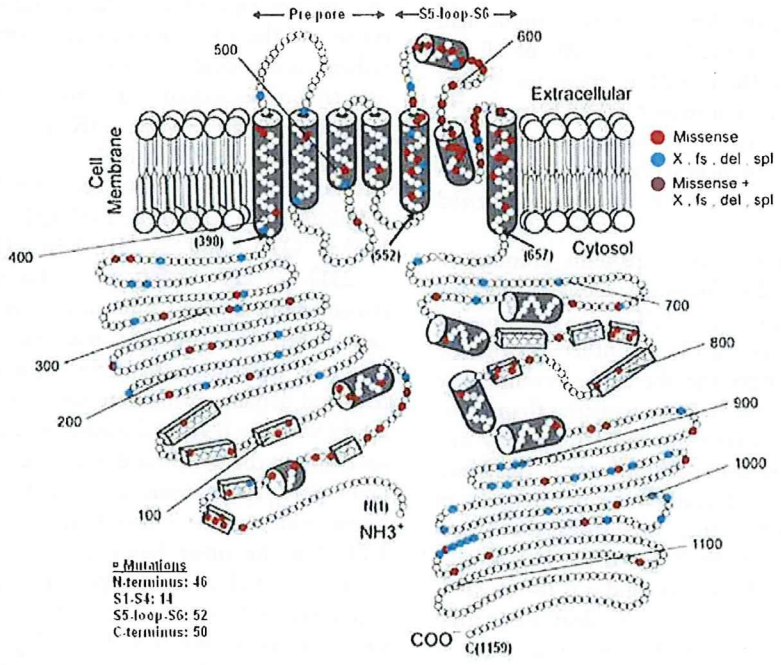

Figure 1 **Location of Different Mutations in KCNH2 Potassium Channel**

Diagramatic location of 162 different mutations in the KCNH2 potassium channel involving 858 subjects. The α subunit involves the N-terminus ($NH3^+$), 6 membrane-spanning segments, and the C-terminus portion (COO^-). The **numbers in parentheses** refer to the position of the amino acid beginning at the N-term position (1), the beginning of the transmembrane nonpore S1 to S4 sequence (398), the beginning of the transmembrane S5-loop-S6 sequence (552), the end of the transmembrane S6 sequence (657), and at the C-term end position (1,159). The **open circles** represent individual amino acids, the **red circles** indicate the missense mutations, and the **blue circles** indicate nonmissense mutations. The **cylinders** represent putative α-helical segments, and the **bars** represent putative β-sheets.

Pre-specified covariate interactions between mutation location, type, and α-helical domains were evaluated. Only the mutation location–missense interaction was significant. To test the impact of the interaction between the 4 different mutation locations and missense mutation type, 3 interaction terms were added to the Cox proportional hazards regression model. A 3 degree of freedom likelihood-ratio test was performed to determine their statistical significance. The influence of time-dependent β-blocker therapy (the age at which β-blocker therapy was initiated) on outcome was determined by adding this variable to the final Cox model containing the various covariates.

Results

Total study population. The continuum of *KCNH2* mutations and their respective number of subjects by location, type, and topology of mutation and contributing registry are presented in the Online Table, and the location, type, and topology of the mutations are diagrammatically presented in Figure 1. A total of 162 different *KCNH2* mutations were identified in 858 subjects. The mutations were predominantly found in 3 regions: the N-terminus (28.4%, n = 46), the C-terminus (30.9%, n = 50), and the transmembrane domain (40.7%, n = 66). Of the 66 mutations within the transmembrane domain, 78.8% (n = 52) were located within the S5-loop-S6 region. Missense (single amino acid substitutions) accounted for 61.7% (n = 100) of all the mutations, splice site for 1.9% (n = 3), in-frame insertions/deletions for 0.6% (n = 1), nonsense for 10.5% (n = 17), and frameshift for 25.3% (n = 41). Sixty-six mutations (40.7%) were located in the α-helical domain, 17 (10.5%) in the β-sheet domain, and 79 (48.8%) in other uncategorized locations.

The phenotypic characteristics of patients enrolled in each of the 4 registries and by location, type, and topology of mutation are presented in Table 1. The age was younger in the Mayo Clinic registry than in the other 3 registries. The QTc interval was longer and the cardiac events were more frequent in the U.S. and Japanese registries than in the other 2 registries. A pacemaker was more frequently implanted in the U.S. registry, and a defibrillator in the Mayo Clinic registry. LQTS-related death was more frequent in the U.S. registry than in the other 3 registries; that seems mainly because the U.S. registry included the largest proportion of patients missing ECG data and was the longest-standing registry, in which 44 of the 92 deaths occurred before 1980. It is not surprising that the death rate in subjects missing ECG data (i.e., QTc) was very high.

Location, type, and topology of mutation on clinical outcome. As to the location of mutation, the QTc interval was longer and cardiac events were more frequent in patients with mutations in the transmembrane pore locations (S5-loop-S6) than in patients with mutations in transmembrane nonpore (S1 to S4), N-terminus, or C-terminus locations. As to the type of mutation, the QTc interval was longer in patients with missense mutations than in patients with either frameshift/nonsense or other mutations. Sudden death was also more frequent among patients with missense mutations. As to the topology of mutation, the QTc interval was longer and cardiac events were more frequent among patients with mutations located in the α-helical domain than among patients with mutations in either the β-sheet domain or other uncategorized location.

The cumulative probabilities of first cardiac event by type, location, and topology of mutation are presented in Figures 2A, 2B, and 2C, respectively. No significant difference in event rates was observed among types of mutation (p = 0.68) (Fig. 2A), although missense mutations were more associated with longer QTc interval and increased risk for sudden death compared with other types of mutations. Conversely, significantly higher event rates were found among subjects with transmembrane pore mutations than among subjects with mutations in transmembrane nonpore, N-terminus, or C-terminus regions, with a gradual increase in event rates occurring during ages 5 to 40 years (Fig. 2B). Significantly higher event rates were also observed among subjects with mutations located in the α-helical domains than among subjects with mutations in either the β-sheet domains or other locations (Fig. 2C).

The findings from the Cox regression analysis by location and by topology of *KCNH2* mutations for first cardiac events and those for aborted cardiac arrest or LQTS-related sudden cardiac death are presented in Table 2. The clinical risk factors associated with first cardiac events involved males before age 13 years (HR: 1.54 vs. females), females after age 13 years (HR: 3.29 vs. males), and longer QTc intervals (HR: 3.33, QTc >530 ms [n = 112] vs. QTc <460 ms [n = 239]; HR: 2.09, QTc 500 to 530 ms [n = 146] vs. QTc <460 ms; HR: 1.56, QTc 460 to 499 ms [n = 251] vs. QTc <460 ms). Mutations located in the transmembrane pore region made significant and independent contributions to the risk model, with C-terminus region as reference (HR: 1.56). Mutations located in the α-helical domains made significant contributions to the risk model with the β-sheet domains as reference (HR: 1.74). A mutation in the α-helical domain located in the transmembrane pore region would have a risk equal to the multiplicative product of the 2 hazard ratios, namely, 1.56 × 1.74 = 2.71. On the other hand, a mutation in the α-helical domain located in the nonpore transmembrane S1 to S4 region would have a risk of 0.61 × 1.74 = 1.06, and this value was very similar to 1. Time-dependent β-blocker use was associated with a significant 63% reduction in the risk of first cardiac events (p < 0.001). The clinical risk factors associated with lethal cardiac events showed similar tendency to those with cardiac events, and involved females after age 13 years (HR: 2.38 vs. males) and longer QTc intervals (HR: 4.97, QTc >530 ms vs. QTc <500 ms; HR: 2.57, QTc 500 to 530 ms vs. QTc <500

Table 1 Phenotypic Characteristics by Source of Subjects, Location of Mutation, Type of Mutation, and Topology of Mutation

	Source of Subjects				Location of Mutation				Type of Mutation			Topology of Mutation		
Characteristics	Rochester	the Netherlands	Japan	Mayo	Transmembrane (S1–S4)	Transmembrane (S5-Loop-S6)	N-Terminus	C-Terminus	Missense	Frameshift/ Nonsense	Others	α-Helices	β-Sheet	Neither
Unique mutations					14	52	46	50	100	58	4	66	17	79
Patients	456	214	95	93	44	259	243	312	555	261	42	319	141	398
Female	57	59	66	57	57	59	56	60	60	56	55	57	55	61
ECG at enrollment														
Age*†‡, yrs	25 ± 20	33 ± 21	30 ± 18	22 ± 16	28 ± 16	24 ± 19	32 ± 21	26 ± 19	28 ± 20	27 ± 19	26 ± 22	25 ± 19	31 ± 22	28 ± 19
QTc*†‡§, s	0.49 ± 0.06	0.47 ± 0.05	0.49 ± 0.05	0.47 ± 0.05	0.48 ± 0.05	0.50 ± 0.06	0.47 ± 0.06	0.48 ± 0.05	0.49 ± 0.06	0.47 ± 0.05	0.47 ± 0.06	0.49 ± 0.05	0.48 ± 0.05	0.48 ± 0.06
QTp*†, s	0.34 ± 0.07	0.33 ± 0.05	0.38 ± 0.06	0.34 ± 0.06	0.37 ± 0.07	0.36 ± 0.07	0.34 ± 0.06	0.34 ± 0.07	0.35 ± 0.07	0.34 ± 0.06	0.34 ± 0.08	0.35 ± 0.07	0.33 ± 0.07	0.34 ± 0.06
Therapy														
β-blockers	51	45	45	60	48	53	45	51	49	51	50	51	48	49
Pacemaker*	6.8	0.5	1.1	0	2.3	6.6	2.5	2.9	4.5	2.7	2.4	5.6	2.8	2.8
Sympathectomy	2	0.9	0	1.1	2.3	1.5	0	2.2	1.6	0.8	2.4	1.6	2.8	0.8
Defibrillator*	14	4.7	6.3	25	18	14	8.2	12	11	13	17	12	9.9	13
First cardiac event*†‡‖	50	34	52	31	34	58	40	38	45	44	29	54	30	41
Syncope*†‡	42	31	52	28	32	49	36	34	39	39	29	45	26	38
Aborted cardiac arrest	0.7	1.9	0	3.2	2.3	1.2	1.2	1	1.3	1.1	0	1.6	0.7	1
Death*†‡	7.7	0.5	0	0	0	7.7	2.9	2.9	5.0	3.1	0	7.2	2.8	2.3
Ever cardiac event														
Syncope*†‡	42	31	55	28	32	49	36	34	39	39	29	45	26	38
Aborted cardiac arrest*	4.6	7.5	16	7.5	11	6.9	6.2	6.7	6.1	8.4	7.1	7.8	4.3	7
Death*†‡§	18	3.3	0	2.2	4.5	17	11	6.7	14	5.7	7.1	16	8.5	7.8

Values are n, %, or mean ± SD. Percentages ≥ 10 are rounded to a whole number. The 858 subjects in this table include 60 subjects from the Rochester-based registry who died suddenly at a young age, were from families with known *KCNH2* mutation, and were assumed to have the family mutation. *p < 0.01 for the comparison of characteristics among the 4 sources of subjects. †p < 0.01 for the comparison of characteristics among the 4 locations of the mutations. ‡p < 0.01 for the comparison of characteristics among the 3 major topologies of mutations. §p < 0.01 for the comparison of characteristics among the 3 major types of mutations. ‖First cardiac event was syncope, aborted cardiac arrest, or sudden death, whichever occurred first.

ECG = electrocardiogram; QTc = corrected QT; QTp = QT peak interval.